Laser enhancements for Lunar Laser Ranging at 532 nm,

G. Martinot-Lagarde, M. Aimar, D. Albanèse, C. Courde, P. Exertier, A. Fienga, H. Mariey, G. Metris, R. Rigard-Cerison, E. Samain, et al.

Results in Physics 6 (2016) 329–336

Contents lists available at ScienceDirect

Results in Physics

journal homepage: www.journals.elsevier.com/results-in-physics

Laser enhancements for Lunar Laser Ranging at 532 nm

G. Martinot-Lagarde [a,*], M. Aimar [a], D. Albanèse [a], C. Courde [a], P. Exertier [b], A. Fienga [b], H. Mariey [a], G. Métris [b], R. Rigard-Cerison [c], E. Samain [a], J.-M. Torre [a], H. Viot [b]

[a] Univ. Nice Sophia Antipolis (UNS), CNRS, IRD, Observatoire de la Côte d'Azur (OCA), Géoazur UMR 7329, 2130 Route de l'Observatoire, 06460 Caussols, France
[b] UNS, UMR 7329, 250 rue Albert Einstein, Sophia Antipolis, 06560 Valbonne, France
[c] Aix-Marseille Université, CNRS (UMR7345), P2IM, Campus Saint-Jérôme, Case 322, Avenue escadrille Normandie-Niemen, 13397 Marseille cedex 20, France

ARTICLE INFO

Article history:
Received 7 April 2016
Accepted 25 May 2016
Available online 15 June 2016

Keywords:
Lunar Laser Ranging
Thermal lensing
Optical design

ABSTRACT

This article exposes how we improved (by more than a factor of four) the green Lunar Laser Ranging instrumental sensitivity of the French telemetric station of the "Observatoire de la Côte d'Azur" in 2012. The primary reason for this success is the doubling of the pulse energy of our green Nd:YAG laser, reaching now 200 mJ at 10 Hz. This first gain is due to the replacement (inside our oscillator cavity) of the dye cell with a CR^{4+}:YAG crystal saturable absorber. Complementary spatial beam profile improvements are also described, regarding polarisation, flashlamp geometry and specific lens arrangements (to exclude ghosts from focusing on the 8 m long amplification chain). Those combined laser enhancements pave the way to future science breakthrough linked to quasi-millimetric determination of the Earth–Moon dynamics (Murphy, 2013). Jointly, we propose an empirical thermal lensing model, varying with the cycle ratio of the flashlamps. Our model connects Koechner's (1970) continuous pumping to our intermittent pumping case, with a "normalised heating coefficient" equalling 0.05 only if the electrical lamp input power is equal to 6 kW and scaling as this [electrical input power into the lamps] to the power of [half the pumping cycle ratio].

Introduction

Lasers are convenient remote sensors of distances, velocities, forces [3] or even chemical agents for various scientific applications ranging from civil engineering to astronomy. In the astronomical field, more than 40 stations realise actively laser ranging on artificial satellites orbiting the Earth (at altitudes from 600 km to 20,000 km) to calibrate the orbits of nearby oceanographic satellites (JASON2 altitude = 1336 km), for spatial geodesy (LAGEOS altitude ~5900 km), for Time Transfer by Laser Links (JASON2\T2L2), for space communications (DOMINO\SOCRATES\SOTA) and for accurate navigation purposes. The International Laser Ranging Service (ILRS), federating astronomical ranging activities, uses the SLR acronym as regards artificial Satellites Laser Ranging to make the difference with this publication scope regarding Lunar Laser Ranging (LLR), accessible to very small number of observatories (<10), and operated on a regular basis by two stations in the world: the US APOLLO station and our French GRSM station, where the 3 first letters of this ILRS code (GRS) are linked to the Grasse sub-prefecture proximity.

Degnan [4] demonstrated millimetric accuracy SLR with two Transportable Laser Ranging Stations (28 cm aperture, 10 mJ) collocated with a MOBLAS station (76 cm aperture, 80 mJ). This leads to the typical SLR station requirements: a 50 cm aperture receiver telescope and a 25 mJ pulsed laser, emitted at 10 Hz, in a $1/e^2$ full angle divergence of 10 arcseconds.

LLR telemetry requires to modify significantly those typical SLR station parameters, as the 380 000 km remoteness of the Moon (compared to LAGEOS 5900 km altitude) generates a telemetric signal attenuation of:

$$[Moon\_range/LAGEOS\_range]^4 \approx [380/5.9]^4 \approx 17 \times 10^6. \quad (1)$$

So, this publication covers our green station progression towards this huge sensitivity gain.

GRSM LLR sensitivity reached in 2012 (compared to the typical SLR case)

Presently, we routinely obtain lunar echoes with a dedicated pulsed laser derived from a QUANTEL cavity and from some THALES(\BMI) components. It delivers green pulses of energy exceeding 200 mJ, with a typical full-angle emission laser divergence of around 1.5 arcseconds (limited by the atmospheric

* Corresponding author.

http://dx.doi.org/10.1016/j.rinp.2016.05.011
2211-3797/

astronomical seeing, being often comprised between 0.5″ and 3″). The GRSM station usually works with a unique telescope (of aperture $\Phi_1 = 154$ cm) guiding alternatively the emitted laser and collecting the echoes, as this maximal aperture configuration is favourable for minimising the footprint of the laser on the Moon.

We stress here that we harvest echoes from 5 flat lunar panels, constituted by sets of corner cubes: 300 for Apollo_15, 100 for Apollo_11 and Apollo_14, and 14 for Lunokhod_1 and Lunokhod_2 (of 11 cm of diameter instead of 3.8 cm). This leads to a mean number of small lunar corner cubes involved for LLR of 147 ($\sim[300 + 100 \times 2 + 14 \times 2 \times (11/3.8)^2]/5$).

LAGEOS satellites also possess many (426) corner cubes of the same diameter as Apollo ones. However, as they are distributed on a sphere (of diameter = 60 cm), the corner cubes facing the station participate more to the return signal than the farther ones. So, for 7 LAGEOS corner cubes participating efficiently to LAGEOS SLR echoes, we get:

$$[Mean\_lunar\_panel/LAGEOS\_sphere]\_reflectivity\_ratio \approx 147/7 = 21. \quad (2)$$

Finally a 9″ tuning of the full angle field of view of our detector damps background lunar diffusions with no LLR signal loss. For SLR, it is usually enlarged to 20″ to facilitate the ranging of low altitude satellites (with speed aberration reaching ~10″ [4]). This procures:

$$[Lunar/LAGEOS]\_detector\_field\_of\_view\_impact \approx (20''/9'')^2 \approx 5. \quad (3)$$

Eqs. (1)–(3) coupled with the typical SLR stations parameter requirements of the introduction give the following Signal Factor (*SF*) from LAGEOS SLR to lunar echoes:

$$SF = ratios\,(laser\_pulse \times emission\_cone \times reflectivity \times collector\_surface \times field \times range^4)$$

$$\Rightarrow$$

$$SF \approx (200/25) \times (10/1.5)^2 \times 21 \times (154/50)^2 \times 5 \times (17 \times 10^6)^{-1} \approx 1/48 \quad (4)$$

As LAGEOS_1 and LAGEOS_2 geodetic satellites fly at an intermediate altitude (~5900 km), each active SLR station is urged to realise ~400 LAGEOS passes per year to derive reliable station coordinates. As only half of those active stations succeeds in ranging towards the farthest 20,000 km orbiting satellites, named HEOs (= High Earth Orbit satellites), we can consider that those HEOs are the farthest targets reachable by typical SLR stations.

We now define a specific Signal to Noise Ratio (named *SNR*), corresponding not to the Individual laser shot Success Rate (*ISR*). Indeed, the *ISR* is tuned below 0.1 (with a motorised attenuator) to remain in the favourable single photon mode regime [5]. In contrast, the *SNR* corresponds to the ratio of the maximum of the time of flight histogram divided by the noise floor, after ~6000 shots. This defines a single experimental point of the lunar orbit called a "normal point". Transposing it to the typical SLR station difficulty to range HEOs gives:

$$Typical\_SLR\_station\_HEOs\_SNR \approx 1, \quad (5)$$

$$(5) \Rightarrow Typical\_SLR\_station\_LAGEOS\_SNR \approx (20000/5900)^4 \approx 132, \quad (6)$$

$$(4) \text{ and } (6) \Rightarrow Mean\_GRSM\_station\_LLR\_SNR \approx 132/48 \approx 2.75 \geqslant 1. \quad (7)$$

This 2.75 GRSM lunar *SNR* value (exceeding 1) explains why our station efficiency increased significantly in 2012 (performing ~4.5 times more Lunar Laser Ranging than in 2011) as shown in the following Table 1. However, this mean LLR *SNR* value of 2.75 also justifies that our success in this green LLR activity still requires a favourable weather, a sufficient Moon elevation ($\geqslant 20°$) and a limited Sun heating of the corner cube panels.

Impact of the atmospheric turbulence on the GRSM station sensitivity

When the sky is very calm, green echoes are lost as soon as we move the telescope away from its best pointing of more than ±0.15 arcseconds. This situation (corresponding to a beam diameter footprint on the Moon of ~553 m) defines an Effective Minimal full-angle Divergence (*EMD*) of the emitted laser beam [6]:

$$EMD \approx 0.3''. \quad (8)$$

In order to confront this *EMD* case to turbulent-free light propagation theory, the full angle Disc_Diffraction_Divergence (*DDD*) of a perfect top-hat emitted beam equals:

$$DDD = 2.44 \times 532\text{ nm} \times 180 \times 3600''/(\pi \times 1.54\text{ m}) = 0.174''. \quad (9)$$

This top-hat model is not directly applicable here, because of our central obstruction (Φ_2/Φ_1) impact. As Ch. André [7] noticed a star brightness dilution $\sim[4''/2.8'']^2 \sim 2$ with a 0.5 central obstruction, we estimate our telescope obstruction impact (10) and turbulent-free gain (11) by:

$$GRSM\_telescope\_obstruction\_impact \approx 1 - \Phi_2/\Phi_1 \approx 1 - 48/154 \approx 0.69, \quad (10)$$

$$Turb.-free\_SNR/EMD\_SNR \approx (1 - \Phi_2/\Phi_1)(EMD/DDD)^2 \approx 0.69 \times (0.3/0.174)^2 \approx 2. \quad (11)$$

In practice, gaining this ultimate lunar signal enhancement densification of (11) remains a difficult task, requiring to damp all atmospheric perturbations of the emitted beam with specific adaptive optics (as adaptive optics are usually designed to improve downward links). So, we will keep this *EMD* case (8) as a reference of our best experimental beam collimation.

Finally, the comparison of this *EMD* case to the usual sky seeing (~1.5″ mentioned in Section 2) authorises a record Lunar_SNR of 70 ($\sim 2.75 \times [1.5''/0.3'']^2$). In practice, our best experimental *SNR* values seldom exceed the 26.677 and 33.743 values (reached in Fig. 1 and in [8]), very likely because we intermittently drift from the ideal pointing during each observation.

In [8], as the Moon field collected by our telescope was not illuminated by the Sun, the noise floor value was very low (~1 single photon) and the number "*n*" of "good echoes" participating to this specific normal point (of the 19 March 2013 at 21H27 UTC) equalled 34.

So, this significant *SNR* value of this first GRSM Lunokhod_1 ranging [8] was very welcome to compensate for its low Individual shot Success Rate (as L1_*ISR* ~ 34/6750 ~ 0.005).

Table 1
2009–2012 LLR normal point statistics, where the low numbers of successful observations in 2009–2010 are due to aperture sharing tests (reducing the link budget).

Annual lunar normal point statistics with the GRSM station at 532 nm	2009	2010	2011	2012
Apollo_11 retroreflector	3	0	6	55
Apollo_14 retroreflector	0	1	16	48
Apollo_15 retroreflector	23	18	60	258
Lunokhod_2 retroreflector	0	0	0	7
TOTAL	26	19	**82**	**368**

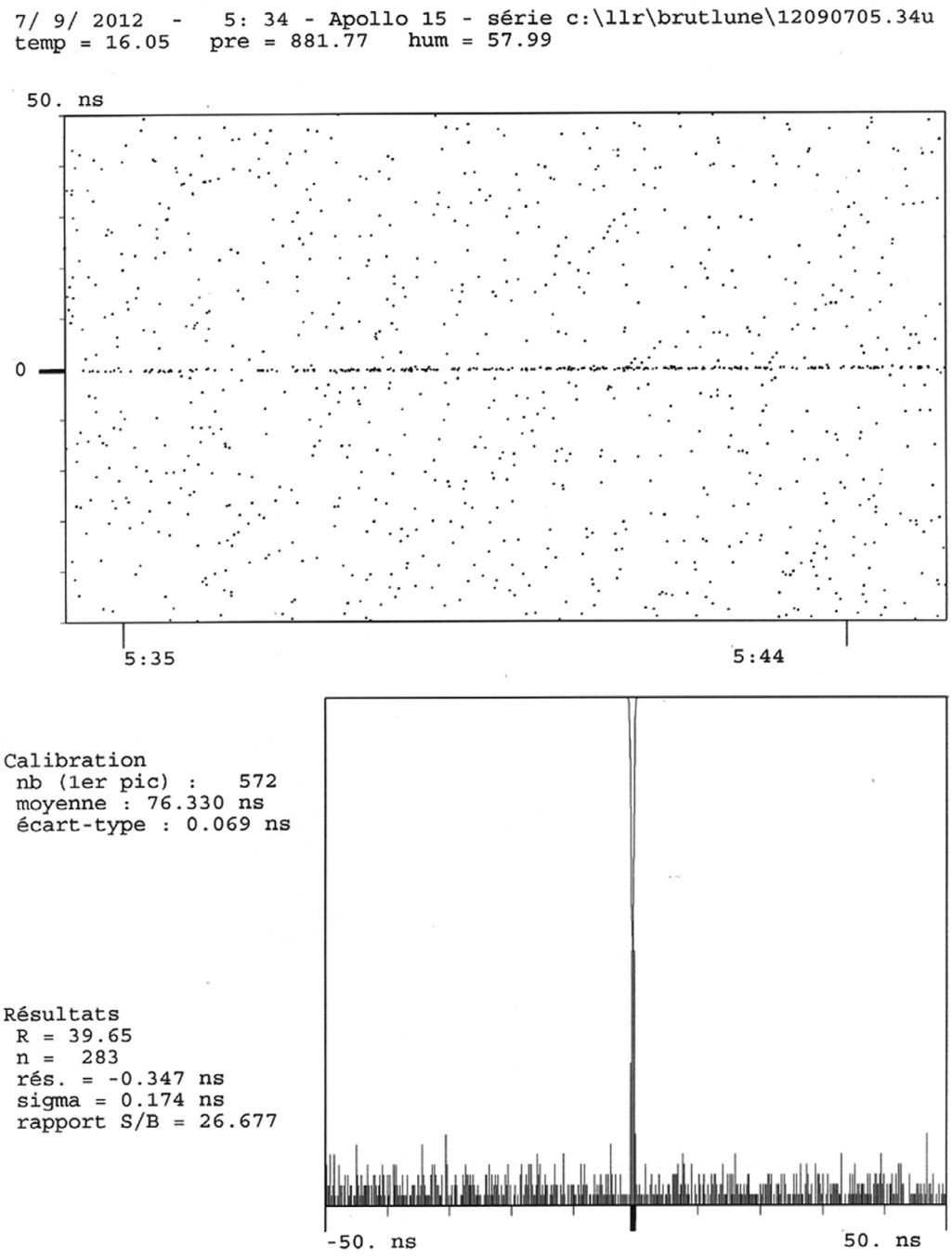

Fig. 1. GRSM normal point built with 283 echoes (the atmosphere being very favourable).

Fortunately, this delicate observing situation is not systematic. Indeed, Fig. 1 shows a much more favourable (Apollo_15) ranging case, where A15_*ISR* ~ 283/6640 ~ 0.04.

Compromise choice for the pulse duration of our GRSM LLR laser

We now point out that the faint energetic level of our lunar echoes (being statistically inferior to a single photon) spreads the statistic of the photon time of flight over the laser pulse length regardless of complementary instrumental or atmospheric uncertainty. So, shortening the pulse length seems to be a convenient way to increase the accuracy of the telemetric results.

However, this shortening also decreases the energy per pulse, due to optical damage threshold limits (or desired to go towards eye-safe laser ranging). So, a repetition rate increase is often implemented (to receive enough echoes) [9]. We recall here briefly this context:

- In 1965, the "Observatoire de Haute Provence" got echoes from the US BEB satellite,
- In 1983, the GRSM station (founded in 1975 by the "CERGA") obtained lunar returns with a Q-switch Ruby laser emitting, every 6 s, a 3 J pulse of 3 ns duration (at 694.3 nm),
- In 1987, a 10 Hz green Nd:YAG laser with 300 mJ pulses of 300 ps replaced the Ruby laser,

- In 1998, E. Samain et al. established the error budget of the GRSM station in [10] and came to the conclusion that a 70 ps laser procures a 350 ps accuracy for each pulse round-trip between the telescope and any Moon retroreflector well oriented towards the earth. Then, an accuracy of 160 ps is estimated in [10] for each LLR normal point. This delivers Apollo_15 panel position (relatively to our station) with a 24 mm accuracy,
- From 2005 to 2011, GRSM LLR were painfully recorded at 10 Hz, with a Nd:YAG laser locked by a dye saturable absorber, with pulses <100 ps, and with a green energy <100 mJ, and
- Since 2012, GRSM LLR is still realised at 10 Hz, but with a pulse duration compromise (of ~150 ps), where the hazardous dye saturable absorber and the 5 m curved mirror of our cavity are replaced by a 4 mm thick MolTech GmbH Cr^{4+}:YAG crystal and by a flat rear mirror. It is important to precise that the fixed (10 Hz) repetition rate of our laser imposes such (~150 ps) laser pulse duration compromise. Indeed, the natural pulse length shortening strategy must be superimposed with our need to accumulate a sufficient number of echoes during our ~6000 shots observing session to validate each observation. So, as the ISR from 200 mJ/150 ps green pulses is significantly higher than the one of the 75 mJ/70 ps laser case of [10]), it happens to be our best experimental configuration.

In this configuration, shown in Fig. 2b, the low minimal transmission of this crystal (~27%) entails that the increase in the lasing threshold (from 1.3 kV to 1.7 kV) is partially limited thanks to an innovative straight-line cavity configuration, contrasting with the right angle beam extraction of Fig. 2a of T. Oldham [11] (requiring an intra-cavity Pockels cell).

This solid laser presents 3 main advantages (already exposed in [11]): a reduced energy jitter (of less than 10%), no more progressive (dye related) beam pointing drift and a maintenance limited by the 4 months flashlamp lifetime (instead of the 3 weeks dye lifetime).

Such stability gains enable us to double the green pulse energy (to 200 mJ) relatively to our unstable dye laser configuration (forcing us to emit output green pulses <100 mJ).

Our 150 ps ± 20 ps Green pulse Full Width at Half Maximum (FWHM), was measured on the 27/01/2012 with a STX 301 event timer. It required reducing the 5 mm Fabry–Perot (FP) thickness to 0.35 mm. As Moblas7 station obtained the same pulse duration with a 1 mm FP thickness [11,12], we conclude that the FP thickness choice is highly cavity dependent.

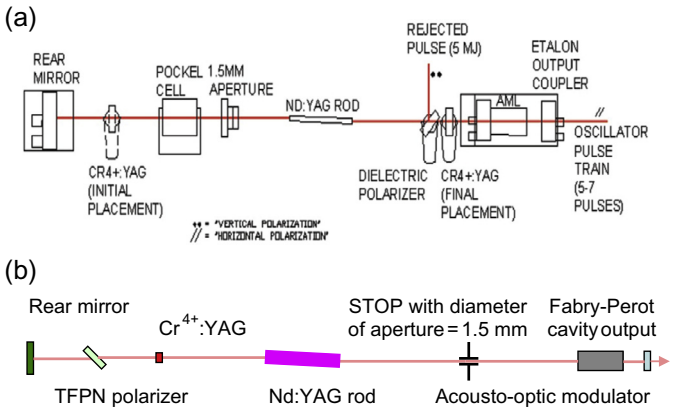

Fig. 2. (a) Moblas 7 cavity where the "REJECTED PULSE" is selected for SLR. (b) GRSM LLR cavity with the [Polariser + Cr^{4+}:YAG crystal] swapped with the [STOP diaphragm] enabling convenient contra-propagating He–Ne pre-alignments.

We must finally add that the deviation to zero of the panel phase angle relatively to the GRSM laser contributes significantly to the error budget. It generates round-trip time dispersion up to 350 ps for Apollo_15 and up to 150 ps for the Lunokhod panels, according to [10]. So, each normal point is degraded by a One way Moon orbit Standard deviation (*OMS*):

$$OMS = 0.5 \times panel\_round - trip\_time\_dispersion\_impact \times Light\_speed \quad (12)$$

$$\Rightarrow \quad Maximal\_Apollo\_15\_OMS = 0.5 \times 350\ \text{ps} \times 3 \times 10^8\ \text{m/s} \approx 53\ \text{mm\_RMS},$$

$$\Rightarrow Maximal\_Lunokhod\_OMS = 0.5 \times 150\ \text{ps} \times 3 \times 10^8\ \text{m/s} \approx 23\ \text{mm\_RMS}.$$

Experimentally, Fig. 1 shows an Apollo_15 round-trip precision of 174ps_RMS and our first GRSM LLR Lunokhod_1 normal point (of the 19 March 2013 at 21H27 UTC) [8] has a round-trip precision of 88ps_RMS. Eq. (12) applied to those experimental precisions confirms that both measurements were done with small panel phase angles. So the resulting *Lunokhod_OMS* value of 13mm_RMS obtained in [8] is a noticeable LLR normal point record.

Finally, we cannot infer straightforwardly that our 200 mJ laser configuration (facilitating Lunokhod normal point obtaining) will lead to a twice better accuracy than the 24 mm one-way accuracy estimated in 1998 in [10], as precision and accuracy are different: the former being estimated by standard deviations and the latter by biases relatively to an "absolute calibration" (issued by a reference experiment, or by a theoretical prediction of the Moon orbit and of the real laser travel through a well characterised atmosphere). Yet, the two models (ELP96 from POLAC or INPOP10e from IMCCE) present a mean discrepancy of 46 mm between their predictions for the 3 days (19–21 March 2013) Lunokhod_1 orbit in [8].

Fortunately, our experimental orbit is located between those models (15 mm away from INPOP10e). So, sub-centimetric LLR ranging [1,10] is now more and more within reach.

Beam profile evolution along the amplifying chain

Fig. 3 (realised with the ZEMAX optical design software) highlights the progressive beam widening along the 3 flash-pumped amplifying rods (A1, A2 and A3) of our GRSM laser. This widening limits the light fluence increase in rods and maximises the pumping efficiency and the beam energy. In practice, the centre of the output face of the biggest rod (A3) is the most stressed surface, with a maximal IR fluence of 0.6 J/cm^2 (with a Gaussian beam assumption).

In Fig. 4, we verified this quasi-Gaussian beam shape (345 mm before A1) with a Laser Beam Profiler (Newport LBP HR [5038]) of 5.2 mm × 6.3 mm active surface. The longest dimension of this active area (defined as "Horizontal" in the LBP software) is oriented along the vertical axis of the laboratory. This analysis is performed with a plane beam-splitter inserted in the main beam path, extracting half its energy towards the LBP sensor (protected by an optical density of 5). There, faint interferences (generated by this plane beam-splitter extractor) are washed out with the [View\Profiles\sum] option choice, realising a summation along each CCD line, procuring each experimental profile (as on the appended black curve).

This footprint matches Gaussian profiles fit with a good correlation factor (>94%). However, we observe a significant vertical ellipticity of this beam (averaged over 4 shots) of:

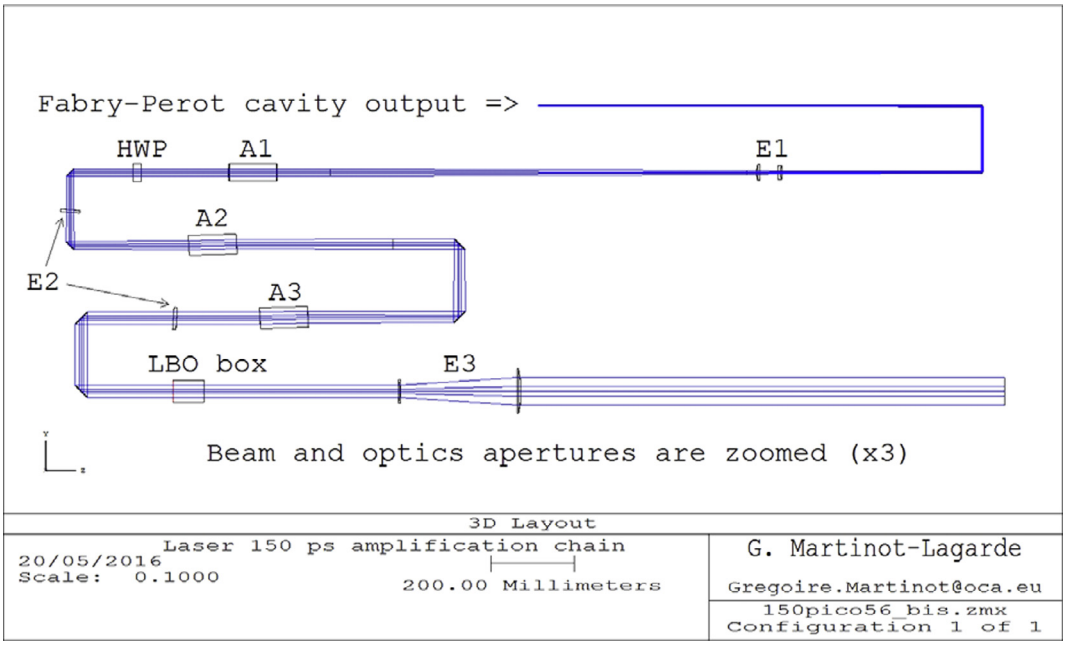

Fig. 3. Top view of the GRSM amplifying chain with 3 E# commercial expanders (comprising 6 plano-spherical lenses of focal lengths = [−92; 150; −1519; 5063; −220; 500] mm), 3 A# amplifiers, a Half-Wave Plate HWP (rotating the laser polarisation of 90°) and a LBO doubler.

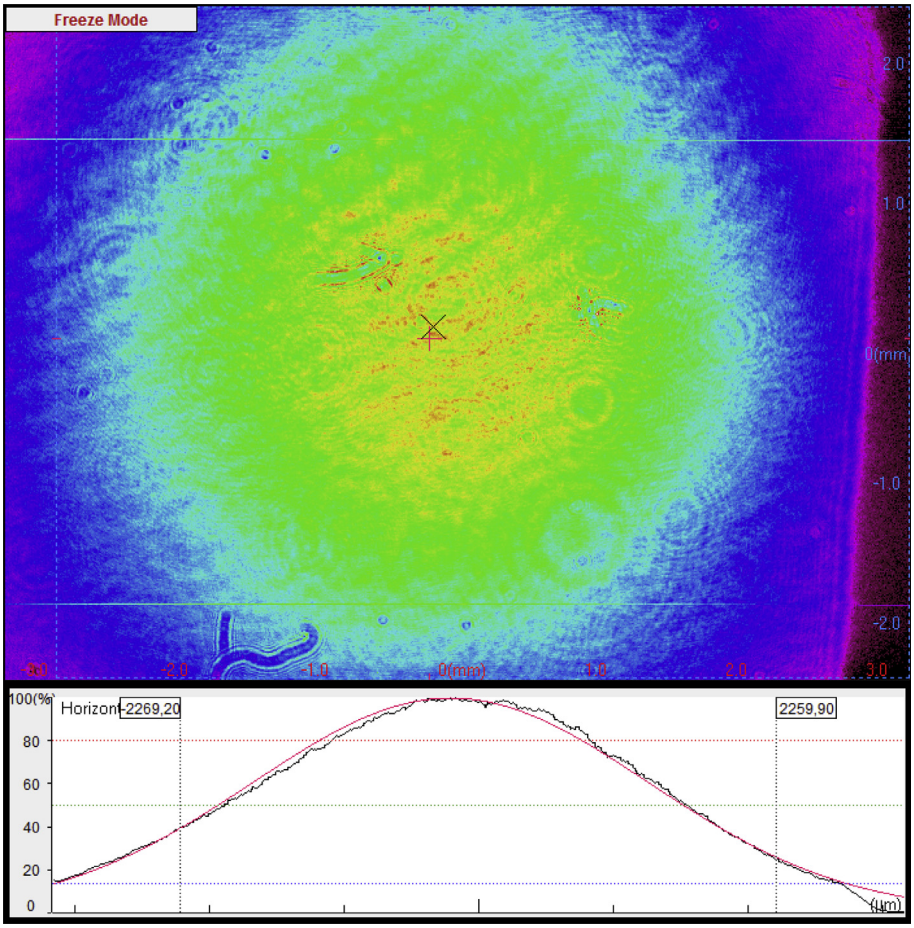

Fig. 4. Black curve = raw beam profile before A1 (deduced from this LBP footprint); red curve = Gaussian fit (showing a $1/e^2$ beam diameter of 6.012 mm).

$$Ellipticity = [5925 + 6012 + 6049 + 5963]/[4905 + 4835 + 4624 + 4683] \approx 1.26 > 1. \quad (13)$$

We then managed to compensate for this local vertical ellipticity (due to polarisation and to flashlamp orientations), by a 90° polarisation tilt (realised by the HWP element of Fig. 3), combined with a 90° rotation of A1 box, to perform a sideway pumping inside A1.

We must add that this beam widening is mainly monitored by the relative positioning of the various lenses of the laser chain, in order to force the beam to fill as much as possible the rod apertures. However, the precaution of excluding any ghost beam from focusing in the beam path is required to assure a correct lifetime for fragile optics (as rods). This led us to:

- reduce the number of lenses on the table from 12 to 6 (reducing the ghosts number),
- exclude backward beam ghosts with a 4° inclination of low power (E2) lenses, and
- reverse the plano-convex lens of the first expander (E1), to protect A2 and A3 rods from a forward ghost beam focus (whose location varies with the tuning of E1).

Experimentally, the appropriate lens choice and positioning does not depend solely on real lens powers, but is also linked to the beamwaist radius of the laser (w_0), to the beam quality factor M^2 and to thermal lensing effects inside the various water-cooled pumped rods.

Practically, as the beam fluence is very high in the vicinity of the cavity waist, we determined this radius (w_0) with comparing the lasing threshold ratio (0.8065) with and without the stop insertion (of radius = w_{STOP} = 0.75 mm) in the CR^{4+}:YAG cavity. As this stop insertion restrains both the beam size and the rod volume interacting with this beam, we applied a square root normalisation to this threshold ratio, leading to:

$$STOP\_transmission = 1 - \exp\left[-2(w_{STOP}/w_0)^2\right] \approx \sqrt{0.8065} \approx 0.9 \Rightarrow w_0 \approx 0.7 \text{ mm}. \quad (14)$$

For the beam divergence, two quality factors $M_x^2 = 1.064$ and $M_y^2 = 1.169$ were measured (where x = horizontal direction and y = vertical one) with the Newport LBP tool (performing similar measurements than in Fig. 4, 3690 mm away from the cavity and with a density = 2).

Table 2 compares our real beam sizes (of col.4) to $1/e^2$ beam radii of the [Zemax\Analysis\Physical_Optics\Paraxial_Gaussian_Beam_Data\Mixed_Mode] tool, with column 5 corresponding to the $M_x^2 = 1.064$ case and with column 6 to the $M_y^2 = 1.169$ one. There, the Nd:YAG crystal (index ~1.8) is replaced by the ZEMAX\N-SF6 glass. Moreover, thermal lensing is emulated by biconvex rods, with effective spherical radius of curvatures ($\pm R_{An}$) defined in Section 6. There, we remark that the radii of column 5 match the mean beam size near A3, and that the values of column 6 emulate better the table exit beam profile (see Fig. 5).

This reveals that the real laser beam suffers a progressive degradation of its quasi-Gaussian profile, building up along the amplification process, with M^2 (= mean quality factor) increasing from ~1.05 to ~1.17. This defines a mean lens worsening of $M^2 \sim [1.17–1.05]/6 \sim 0.02$. Transferring this ZEMAX analysis at the output of our 2011 laser (with a dye cavity and 12 lenses) procures $M^2_{dye} \sim [1.2 + 12 \times 0.02] \sim 1.44$. So, our enhanced green laser should procure a laser footprint densification on the Moon of

$$[M^2_{dye}/M^2]^2 \approx (1.44/1.17)^2 \approx 1.5. \quad (15)$$

Generalised Nd:YAG thermal lensing formalism

A detailed study of thermal lensing inside a pulsed Nd:YAG rod was performed by Eichler et al. in 1993 [13]. The authors showed that thermal lensing could be considered in a steady state for repetition rates higher than 5 Hz (with 80 J/pulse of pump energy). This corresponds well to our 10 Hz repetition rate situation. Moreover, they found that average electrical pump power P drives this thermal lensing effect. Finally, they measured a quasi-linear dependence between this pumping power (P) and their pulsed thermal lensing.

This result differs from Koechner's [2] measurements (reproduced on Fig. 6) inside a continuously pumped rod of radius $r_0 = 3.1$ mm, where his two theoretical polarised dependent thermal focal lengths ($f_1 = 1.41$ m kW/P and $f_2 = 2$ m kW/P) are averaged experimentally to:

$$AFL_{Refined\ \ Koechner}/1kW \approx [2/(1/f_1 + 1/f_2)]\ /\sqrt{P/P_K} \approx 1.65\,\text{m} \times P_K^{0.5}/P^{1.5}, \text{ with } P_K = 6\,\text{kW}. \quad (16)$$

Independently, Stuart [14] established that laser induced damage fluence scales with the square root of the pulse width duration (for pulse durations >100 ps). There, two pulse durations τ_A, τ_B

Table 2
Beam size evolution along the laser table.

Beam size evolution along the laser table	z_n = thickness of surface "n" from the cavity output (mm)	*Experimental method of measurement of the beam profile* or mechanical rod radius ($r_{1,2,3}$)	Experimental beam radius measurements (mm)	ZEMAX $1/e^2$ physical optics beam radius where $M_x^2 = 1.064$ (mm)	ZEMAX $1/e^2$ physical optics beam radius where $M_y^2 = 1.169$ (mm)
Cavity output (= Fabry–Perot FP)	$z_5 = 0$	w_{STOP} = 0.75 mm *and* T_stop = 0.9	(14) ⇒ 0.7	0.7	0.7
After E1	$z_{23} = 1786$	*Digital calliper*	1.8 ± 0.2	1.749	1.859
Before rod_A1	$z_{25} = 2786$	*Digital calliper*	2.9 ± 0.3	3.225	3.446
rod_A1 output	$z_{32} = 3030$	$r_1 = 3.5$ mm		3.469	3.709
After rod_A1	$z_{34} = 3260$	*Thermal paper*	3.2 ± 0.3	3.507	3.752
Laser Beam Profiler (LBP)	$z_{LBP} = 3690$ of free space travel	$1/e^2$ LBP *horizontal diameters* (x axis) = {3.936; 4.059; 4.149}	$1/e^2$ LBP vertical *diameters* (y axis) = {4.419; 4.419; 4.368}	Free space mean horizontal radius = 2.024	Free space mean vertical radius = 2.201
rod_A2 output	$z_{52} = 3990$	$r_2 = 4.76$ mm		4.488	4.808
After rod_A2	$z_{56} = 4365$	*Thermal paper*	4.8 ± 0.5	4.982	5.340
rod_A3 output	$z_{68} = 5179$	$r_3 = 6.35$ mm		5.967	6.401
After rod_A3	$z_{77} = 5483$	*Thermal paper*	6.05 ± 0.6	6.057	6.498
Table exit	$z_{96} = 8000$	*Thermal paper*	13.5 ± 1.3	12.61	13.54

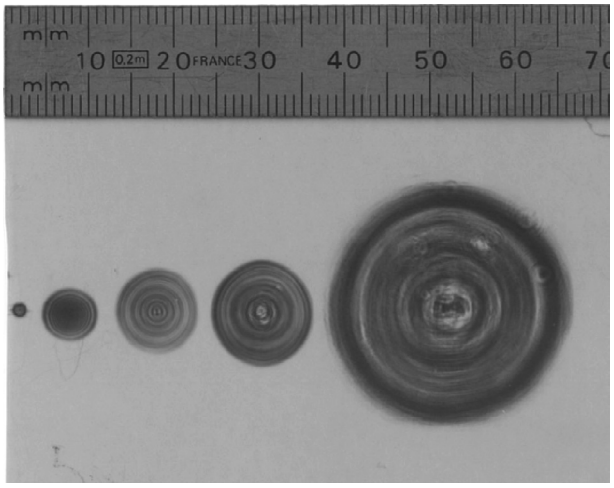

Fig. 5. Thermal footprints showing the progressive widening of the beam along the laser chain: – before A1, after A1, (where the slight horizontal ellipticity of this 6 mm diameter footprint is due to the left and right sides pumping in A1) after A2, after A3, and after E3.

associated with damaging optical fluences E_A, E_B generating equivalent damages (corresponding to a damaging energy H) procure a heating coefficient evolution of:

$$\eta_B/\eta_A = [H/E_B]/[H/E_A] \approx \sqrt{\tau_A/\tau_B} \approx [E_B/E_A] \times [\tau_A/\tau_B] = P_B/P_A. \quad (17)$$

This optical damage case [14] is more severe than our non-destructive flashlamp pumping. However, Eq. (17) significant variation of the heating coefficient ($\eta_{A,B}$) with the instantaneous pulse power ($P_{A,B}$) makes us realise that our heating coefficient ($\eta \sim \eta_K = 0.05$), converting our average electrical pump power P into rod heating, might also increase with P.

So, for a Nd:YAG rod An (of radius r_{An}) pumped by two lamps (with P) at a cycle ratio h, we propose to extend the Average thermal Focal Length of (16) to any value of $h \in]0;1]$ with:

$$AFL/1\text{ kW} = (r_{An}/r_0)^2 \times (1.65\text{ m}/P)/(\eta/\eta_K); \quad \text{with} \quad \eta/\eta_K = (P/6\text{ kW})^{h/2} \quad (18)$$

$$\Rightarrow \quad \eta/\eta_K \sim 1 \quad \text{for our three first rods A0, A1 and A2 (as } h \sim 0.002 << 1). \quad (19)$$

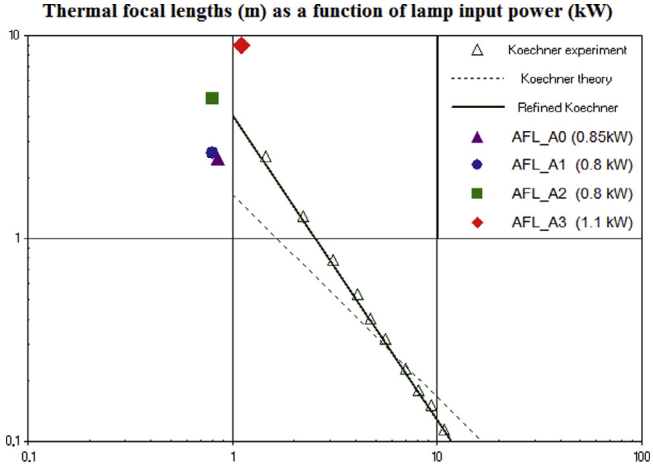

Fig. 6. GRSM Average thermal Focal Lengths of (24–27) superimposed with those of [2].

We observed that A3 rod (being surrounded by 4 flashlamps instead of 2) presents a reduced thermal lensing. Paugstadt and Bass [15] studied temperature profiles inside a ErTmHo:YAG rod (of radius 2.5 mm) illuminated by a unique flashlamp, placed 10 mm under the rod. They measured a significant overheating (>1°) on the rod shell facing this flashlamp, being progressively transferred to the rod centre. This indicates that the more homogenous pumping of A3 (relatively to the other rods) is likely to smooth its temperature profile. So, η' will replace the coefficient η of (18) for A3 thermal lensing calculation with:

$$\eta' \approx 0.7\eta. \quad (20)$$

$$\text{Eqs. (18, 19)} \quad \Rightarrow AFL_{An}/1kW \approx (r_{An}/r_0)^2 \times 1.65\text{ m}/P \quad \text{for} \quad n \in \{0;1;2\} \quad (21)$$

$$\text{and Eqs. (18, 20)} \quad \Rightarrow AFL_{A3}/1kW \approx (r_{A3}/r_0)^2 \times 1.65\text{ m}/(0.7P) \quad (22)$$

$$\text{with } r_{A0} = r_{A1} = r_1 = 3.5\text{ mm}, \quad r_{A2} = r_2 = 4.76\text{ mm}, \quad r_{A3} = r_3 = 6.35\text{ mm} \quad \text{and} \quad r_0 = 3.1\text{ mm}. \quad (23)$$

Finally, as $[I_{flashlamp\ pair} = 1kW/2kV = 0.5A]$ and as $[R_{An} \approx 1.54 \times AFL_{An}]$, we get:

$$V_{A0} = 1.7\text{ kV} \quad \Rightarrow \quad P_{A0} = I \times V_{A0} = 0.85\text{ kW} \quad \Rightarrow \quad AFL_{A0} \approx 2474\text{ mm} \quad \Longleftrightarrow \quad R_{A0} \approx 3810\text{ mm}, \quad (24)$$

$$V_{A1} = 1.6\text{ kV} \quad \Rightarrow \quad P_{A1} = I \times V_{A1} = 0.8\text{ kW} \quad \Rightarrow \quad AFL_{A1} \approx 2629\text{ mm} \quad \Longleftrightarrow \quad R_{A1} \approx 4049\text{ mm}, \quad (25)$$

$$V_{A2} = 1.6\text{ kV} \quad \Rightarrow \quad P_{A2} = I \times V_{A2} = 0.8\text{ kW} \quad \Rightarrow \quad AFL_{A2} \approx 4863\text{ mm} \quad \Longleftrightarrow \quad R_{A2} \approx 7489\text{ mm}, \quad (26)$$

$$V_{A3} = 800\text{ V} + (100\text{ V}/scale\,unit) \times [BMI\ vernier\ value\ of\ 3] = 1.1\text{ kV},$$

$$\Rightarrow P_{A3} = 2I \times V_{A3} = 1.1kW \quad \Rightarrow \quad AFL_{A3} \approx 8991\text{ mm} \quad \Longleftrightarrow \quad R_{A3} \approx 13,846\text{ mm}, \quad (27)$$

where $\pm R_{An}$ is the rod faces radius of curvature emulating An thermal lensing (with ZEMAX).

Conclusion

This study is focused on pulsed laser developments for the GRSM Lunar Laser Ranging station. Firstly, a comparison of our station parameters to LAGEOS ranging enables us to define our actual averaged LLR Signal to Noise Ratio of 2.75; where exceptional (or unfavourable) observing conditions improve (or degrade) it by an order of magnitude.

Then, the central scope of this study consists in describing several enhancements of our pulsed laser, in order to explain why we obtained an impressive LLR normal point productivity gain of the factor 4.5 between 2011 and 2012. We can conclude now that:

- our pulse energy doubling is responsible for a LLR sensitivity gain of [2/4.5] = 44%,
- beam shape upgrades add a 33% contribution (through a Moon beam densification of 1.5), and
- lastly, our triple reliability enhancement (in energy stability, in pointing and in maintenance relief) share the remaining 33% responsibility for our productivity gain.

Finally, as our enhanced laser design was contingent on rods thermal lensing, we established a generalised Nd:YAG thermal

lensing formalism (18–20), being consistent with 4 complementary heat transfer situations [2,13–15]. As this approach describes well our (8 m long) amplifying chain propagation, we advise it to optimise solid-state laser integrations in optical designs (for laser ranging, optical tweezers, lidars, high energy physics...).

Appendix A. Supplementary data

Supplementary data associated with this article can be found, in the online version, at http://dx.doi.org/10.1016/j.rinp.2016.05.011.

References

[1] Murphy TW. Lunar laser ranging: the millimetre challenge. Rep Prog Phys 2013;76. http://dx.doi.org/10.1088/0034-4885/76/7/076901. 076901 (21pp).
[2] Koechner W. Thermal lensing in a Nd:YAG laser rod. Appl Opt 1970;9 (11):2548–53.
[3] Martinot-Lagarde G. Eur J Phys 1995;16:282–3.
[4] Degnan JJ. Millimeter accuracy satellite laser ranging: a review. In: Contributions of space geodesy to geodynamics: technology, Geodynamics, vol. 25; 1993. p. 133.
[5] Nicolas J et al. Appl Opt 2000;39(3):402–10.
[6] Burris R, et al. In: 18th ILRS workshop, Tokyo, Japan; 2013; 8: 13-03-06-Burris.pdf.
[7] André Ch. Ann. de l'Ec. Normale 2e Série, vol. 5; 187. p. 336.
[8] Torre J-M,. et al. Journal of Geodesy, . First LLR observations of Lunokhod 1 with MéO instrument (Calern, France). In: (accepted); leading to results exposed at the 18th ILRS workshop, Tokyo, Japan, Journal of Geodesy, special ILRS, vol. 9; 2013. 13-04-03-Bouquillon.pdf.
[9] Kirchner G, Koidl F. In: 14th ILRS workshop, Spain; 2004. Session AST: adv4_gkm.pdf.
[10] Samain E et al. Astron Astrophys Suppl Ser 1998;130:235–44.
[11] Oldham T, et al. In: 16th ILRS workshop, Poznan, Poland, vol. 7; 2004. las_7_Oldham_p.pdf.
[12] Desch N. 2012 http://ilrs.gsfc.nasa.gov/network/stations/active/YARL_sitelog.html.
[13] Eichler HJ et al. Thermal lensing and depolarization in a highly pumped Nd:YAG laser amplifier. J Phys D: Appl Phys 1993;26:1884–91.
[14] Stuart BC et al. Laser-induced damage in dielectrics with nanosecond to subpicosecond pulses. Phys Rev Lett 1995;74:2248–51. 0031-9007/95/74 (12)/2248(4).
[15] Paugstadt R, Bass M. Method for temporally and spatially resolved thermal lensing measurements. Appl Opt 1994;33(6):954–9.